Chapter 5: Synthesis and Characterization of Bimetallic Rh(III)-Pt(II) DNA Mismatch Binding Complexes with Bridging Intercalator Ligands

5.1 Introduction

The development of rhodium metalloinsertors, which target thermodynamically destabilized base pair mismatches in DNA with high specificity and affinity, into bifunctional conjugates has long been a focus of the Barton laboratory. The appendage of functionalities with various biological activities to these mismatch recognition complexes affords unique compounds with dual functionalities, often enabling the targeting of otherwise nonselective compounds towards mismatched DNA.[1-4] A primary focus in the design of bifunctional metalloinsertor conjugates is the incorporation of cytotoxic, DNA crosslinking platinum (II) moieties.[3,5] Platinum chemotherapeutics are employed in the treatment of over 50% of all cancers and have been widely successful in the treatment of several malignancies.[6-10] However, single-agent therapy is increasingly uncommon, and even common chemotherapeutics like cisplatin are typically administered in conjunction with one or more drugs, each functioning separately but synergistically within the cell.[11] We have expanded the notion of combination therapy further, in the employment of cell-specific rhodium metalloinsertors that may function not simply as separate synergistic adjuvants, but rather as conjugated targeting agents for platinum. The ability to direct these agents towards lesions in DNA associated with carcinogenesis would be a significant enhancement in the development of targeted therapies.[12]

Several examples of metalloinsertor-platinum conjugates have already been characterized.[3,5,13] Each generation of Rh-Pt complex is unique in its construction and biological activity. The first-generation conjugate, developed over ten years ago, involves

a trisheteroleptic Rh(chrysi)(phen)(bpy')]$^{3+}$ metalloinsertor scaffold, where bpy' is a 2,2'-bipyridine ligand modified with an amino-alkane linker, chrysi (5,6-chrysenequinone diimine) is the sterically expansive inserting ligand for mismatch recognition, and phen (1,10-phenanthroline) serves as an additional ancillary ligand. The rhodium complex was functionalized with a cisplatin derivative via the non-leaving group ligand and was found to enhance the formation of covalent platinum adducts preferentially at mismatched DNA, provided that the preferred d(GpG) binding site was adequately accessible within the constructs of the alkyl tether.[3]

The structural limitations of the first-generation Rh-Pt conjugate bore biological consequences. Despite the targeted platination of mismatched DNA *in vitro*, the complex was unable to successfully inhibit proliferation in mismatch repair (MMR)-deficient cancer cells, instead targeting the isogenically matched MMR-proficient cell line, much like its cisplatin parent complex.[14,15] This preferential targeting of MMR-proficient cells can be a potentially devastating side effect of chemotherapy, as the deleterious effects of the MMR-deficiency phenotype are allowed to further proliferate. Selection for MMR-defects resulting from chemotherapy-induced DNA damage is a major cause of secondary leukemias and other malignancies.[16]

The second-generation Rh-Pt complex addressed these issues: here, the platinum subunit was attached to the rhodium complex not through its inert ammine ligand, but rather through the labile leaving group.[5] This afforded a temporary linkage between the rhodium and platinum subunits, with the intention of the conjugate remaining intact long enough for the metalloinsertor to taxi its cargo to mismatched DNA. This design strategy enabled the platinum subunit to bind DNA regardless of the location of the d(GpG) site.

In this second-generation conjugate, we employed an oxaliplatin derivative, which is active in MMR-deficient cancers, rather than the cisplatin analogue of the previous conjugate. We also replaced the lipophilic phen and bpy' ligands with ligands derived from HDPA (2,2'-dipyridylamine), a flexible, hydrophilic ligand that has been shown to display accelerated cellular uptake and selective biological activity.[17-19] Based on previous studies establishing that highly lipophilic ligands are unfavorable for cell-selective targeting of MMR-deficiency due to uptake into mitochondria,[19,20] elimination of the greasy alkyl chain was anticipated to enhance biological efficacy in addition to eliminating the sequence dependence of the previous complex.

This new strategy proved successful in some aspects of its design: the hydrophilic complex was able to remain intact during cellular uptake and localization to the nucleus, while displaying minimal mitochondrial sequestration. This resulted in a 3-fold enhancement in potency in MMR-deficient cells over cisplatin as well as oxaliplatin, the FDA-approved first line therapy for colorectal cancers. However, this potency was not selective for MMR-deficient cells, although the conjugate did target both cell lines equally rather than mimicking the reverse-selectivity displayed by the previous complex. Additionally, the hydrolysable construct abolished preferential targeting of mismatched DNA by platinum, resulting in the formation of Pt-DNA adducts with both mismatched and well-matched DNA.[5]

In addition to these published examples, several other iterations of bimetallic conjugates have been explored for mismatch-directed targeting of platinum.[13,21] However, in all of these cases, the metalloinsertor was functionalized via attachment of the platinum subunit (or other cargo) to one of the non-inserting ancillary ligands. This

approach has the advantage of ligand modulation with relative synthetic ease, in addition to leaving the chrysi ligand unmodified for insertion into the nucleobase π-stack; however, the appendage of potentially bulky cargo extending from the back of the metalloinsertor has the potential to interfere with DNA binding affinity,[3] or possibly *in vivo* recognition and processing of the metalloinsertor-bound DNA lesion. As a result, conjugation of cargo from the ancillary ligands of metalloinsertors can lead to unforeseen biological consequences.

Here, we present an approach to bimetallic Rh(III)/Pt(II) mismatch recognition complexes previously unexplored in our laboratory. Instead of connecting the two metal centers via the metalloinsertor ancillary ligands, we have synthesized a new inserting ligand capable of chelating both metal centers directly. Thus, there is no modular linker region between the two metal centers; rather, the ligand is modified with additional coordination sites for the direct chelation of platinum. In this way, metalloinsertion and platination are intrinsically linked, as insertion into a mismatched site would place the platinum center directly into the DNA lesion (**Figure 5.1**). Within this model, both of the ancillary ligands can potentially be varied to enhance DNA binding affinity and biological efficacy. Two complexes have been synthesized (**Figure 5.2**), $[(bpy)_2Rh(\mu\text{-phendione})PtX_2]^{3+}$ and $[(bpy)_2Rh(\mu\text{-bzp})PtX_2]^{3+}$ (bpy = 2,2'-bipyridine; phendione = 1,10-phenanthroline-5,6-dione; bzp = benzo[*b*][1,10]phenanthroline-5,6-dione; X = labile leaving group ligand (Cl, H_2O)), with the phendione and bzp ligands coordinating to both rhodium (*via* the imines) and platinum (*via* the distal nitrogens). In the case of $[(bpy)_2Rh(\mu\text{-phendione})PtX_2]^{3+}$, the phendione ligand is capable of metalloinsertion at the site of a mismatch, but is also narrow enough to intercalate into well-matched DNA. The

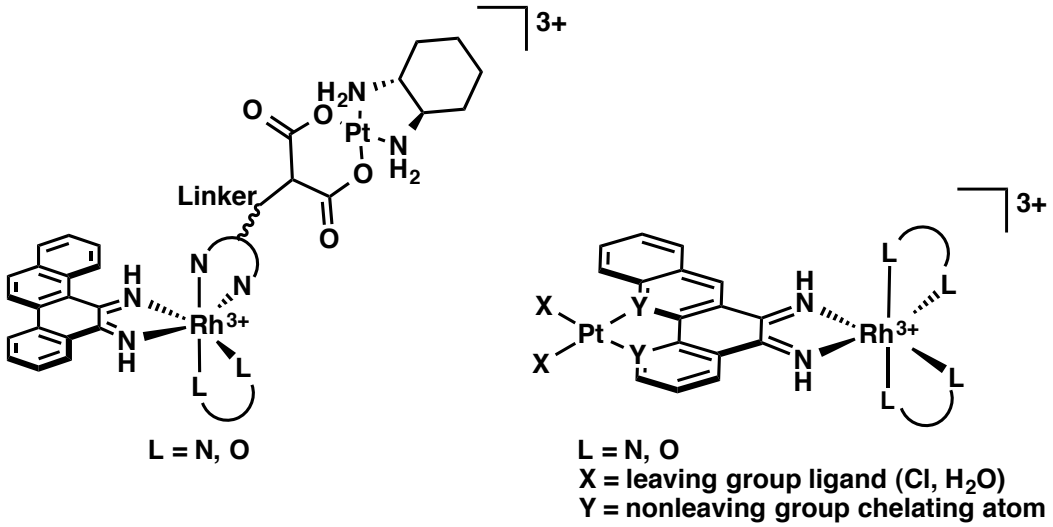

Figure 5.1 General structures of two distinct families of Rh-Pt metalloinsertor conjugates. Left: the non-inserting ancillary ligands are modified with therapeutic cargo; Right: the second metal directly chelates to the inserting ligand via a distal coordination site opposite the Rh(III) center.

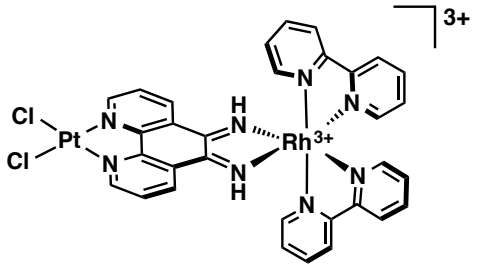

$[(bpy)_2Rh(\mu\text{-phendione})PtCl_2]^{3+}$

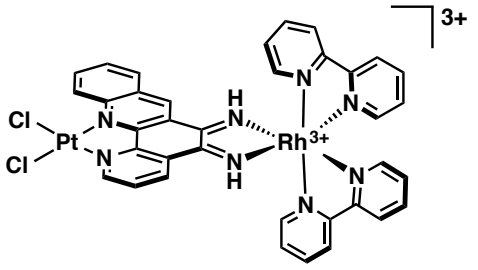

$[(bpy)_2Rh(\mu\text{-bzp})PtCl_2]^{3+}$

Figure 5.2 Chemical structures of two mixed-metal Rh(III)/Pt(II) metalloinsertor complexes, wherein both metal centers are coordinated to the bridging aromatic ligand that interacts with the DNA base stack. Left: $[(bpy)_2Rh(\mu\text{-phendione})PtCl_2]^{3+}$, where phendione (1,10-phenanthroline-5,6-dione) is an intercalating ligand that can bind at mismatched or well-matched sites; Right: $[(bpy)_2Rh(\mu\text{-bzp})PtCl_2]^{3+}$, where bzp (benzo[*b*][1,10]phenanthroline-5,6-dione) is a sterically expansive analogue of phendione designed to selectively target destabilized mismatches. The platinum centers also contain two *cis*-labile chloride ligands that are hydrolyzed under aqueous conditions to form covalent DNA crosslinks.

complex also forms platinum crosslinks with mismatched and well-matched DNA. The $[(bpy)_2Rh(\mu\text{-bzp})PtX_2]^{3+}$ complex was synthesized with the intention of being a mismatch-specific analogue to $[(bpy)_2Rh(\mu\text{-phendione})PtX_2]^3$. The bzp ligand appears to be theoretically too wide to intercalate into well-matched DNA, but inserts at mismatched sites. This complex displays two distinct binding modes that depend on whether the complex is interacting with DNA containing a thermodynamically destabilized site.

5.2 Experimental Protocols

5.2.1 Materials

All organic reagents were purchased from Sigma-Aldrich unless otherwise noted. Commercially available chemicals were used as received without further purification. $RhCl_3$ and K_2PtCl_4 starting material were purchased from Pressure Chemical Co (Pittsburgh, PA). Sep-pak C_{18} solid-phase extraction (SPE) cartridges were purchased from Waters Chemical Co. (Milford, MA).

Oligonucleotides were ordered from Integrated DNA Technologies and purified by HPLC using a C18 reverse-phase column (Varian, Inc; Corona, CA). All HPLC purifications were carried out on a Hewlett-Packard 1100 HPLC. DNA purity was confirmed by MALDI-TOF mass spectrometry and quantified by UV-visible spectroscopy (UV-vis) using the extinction coefficients at 260 nm estimated for single-stranded DNA. UV-vis characterizations were performed on a Beckmann DU 7400 spectrophotometer. Radiolabeled [^{32}P]-ATP was purchased from MP Biomedicals (Santa Ana, CA).

The synthesis of $[Rh(bpy)_2(NH_3)_2]^{2+}$ was carried out according to literature procedures.[17]

5.2.2 Ligand Synthesis

5.2.2.1 Synthesis of 5,6-dihydrobenzo[*b*][1,10]phenanthroline (Scheme 5.1)

A 250 ml roundbottom flask was charged with 6,7-dihydroquinoline-8(5*H*)-one (147 mg, 1 mmol) and 2-aminobenzaldehyde (121 mg, 1 mmol) in 30 ml EtOH. A solution of KOH (151 mg, 2.7 mmol) in 5 ml EtOH was added, and the solution was heated at reflux for 24 h. After cooling to room temperature, the solvent was removed *in vacuo*, and the residue was partitioned between dichloromethane and water. The organic phase was extracted with water (3 x 50 ml), washed with brine, and dried over $MgSO_4$. The crude product in CH_2Cl_2 was filtered through a plug of Al_2O_3, washing with CH_2Cl_2 to afford the pure product in quantitative yield (233 mg). ESI-MS (cation): *m/z* calc. 233 ($M+H^+$), obs. 233.1. ^{1}H NMR (500 MHz, $CDCl_3$) δ 8.84 – 8.81 (m, 1H), 8.41 – 8.37 (m, 1H), 8.00 (s, 1H), 7.80 – 7.74 (m, 1H), 7.68 (ddd, *J* = 8.5, 6.8, 1.5 Hz, 1H), 7.62 (dq, *J* = 7.6, 0.9 Hz, 1H), 7.52 (ddd, *J* = 8.2, 6.9, 1.2 Hz, 1H), 7.29 (dd, *J* = 7.6, 4.7 Hz, 1H), 3.18 (dd, *J* = 8.4, 5.7 Hz, 2H), 3.06 (dd, *J* = 8.4, 5.6 Hz, 2H).

5.2.2.2 Synthesis of benzo[*b*][1,10]phenanthroline-5,6-dione ("bzp") (Scheme 5.2)

To a solution of 5,6-dihydrobenzo[*b*][1,10]phenanthroline (233 mg, 1 mmol) in 1:1 glacial acetic acid:acetic anhydride (10 ml) was added sodium dichromate (524 mg, 1.76 mmol) in 1:1 AcOH:Ac_2O (10 ml) dropwise at 0 °C. The reaction was allowed to stir for 8 days, followed by dilution with water (50 ml) and neutralization with saturated aqueous sodium bicarbonate. The mixture was extracted in 75 ml portions with dichoromethane (4 x 50 ml), and the organic fractions were pooled and dried over

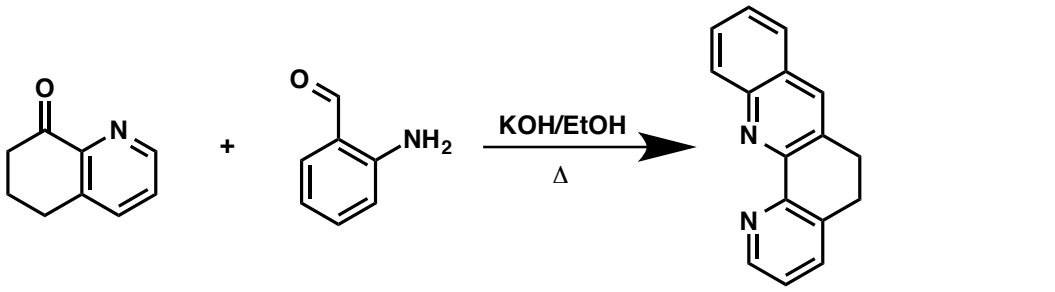

5,6-dihydrobenzo[*b*][1,10]phenanthroline

Scheme 5.1 Synthesis of 5,6-dihydrobenzo[*b*][1,10]phenanthroline.

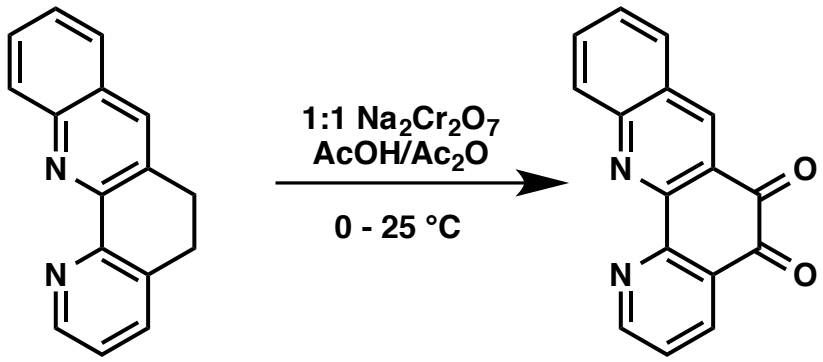

benzo[*b*][1,10]phenanthroline-5,6-dione

Scheme 5.2 Synthesis of benzo[*b*][1,10]phenanthroline-5,6-dione ("bzp"), which contains two bidentate chelating systems: the di-quinone will condense with $[Rh(bpy)_2(NH_3)_2]^{3+}$, while the phenanthroline nitrogens serve as the platinum ligand.

$MgSO_4$. The solvent was removed *in vacuo*, and the ligand, benzo[*b*][1,10]phenanthroline-5,6-dione ("bzp") was used without further purification. ESI-MS (cation): *m/z* calc 261 ($M + H^+$), obs. 261.

5.2.3 Synthesis of Metal Complexes

5.2.3.1 [$PtCl_2$(phendione)] (Scheme 5.3)

The synthesis of [$PtCl_2$(phendione)] was carried out as described in the literature, with minor modifications.[22] 1,10-phenanthroline-5,6-dione ("phendione," 50.6 mg, 0.24 mmol) in 20 ml EtOH was added dropwise to a solution of potassium tetrachloroplatinate (100 mg, 0.24 mmol) in 20 ml water in the dark. The mixture was heated to 50 °C for 24 h and filtered. The precipitate was washed with cold ethanol (3 x 5ml), and diethyl ether (3 x 5 ml), and the resulting green-brown solid was dried under vacuum. Yield: 91 mg (80%) ^{1}H NMR (500 MHz, DMSO-d6) δ 9.53 (m, 2H), 8.91 – 8.56 (m, 2H), 8.18 – 7.86 (m, 2H). ESI-MS (anion): *m/z* calc 476 ($M - H^-$), *m/z* obs. 475.1, 477.1

5.2.3.2 [$(bpy)_2Rh(\mu\text{-phendione})PtCl_2]^{3+}$ (Scheme 5.4)

[$Rh(bpy)_2(NH_3)_2$]OTf_3 (83.5 mg) was dissolved in 30 ml 5:1 MeCN/H_2O. $PtCl_2$(phendione) (55.7 mg, 1.26 eq) was added, and the mixture was sonicated until the platinum was dissolved. NaOH (2 ml, 1 N) was then added, and an immediate color change to red-orange occurred. The reaction was stirred at room temperature in the dark for 24 h and subsequently dried *in vacuo*. The crude product was redissolved in a minimal volume of H_2O and purified by reverse-phase HPLC (85:15:0.1 to 40:60:0.1 H_2O/MeCN/TFA gradient). ^{1}H NMR (500 MHz, D_2O): δ 9.69 (ddd, J = 5.7, 1.5, 0.7 Hz, 1H), 9.11-9.06 (m, 1H), 8.64-8.59 (m, 2H), 8.51-8.49 (m, 1H), 8.47 (tdd, J = 8.0, 2.5, 1.5

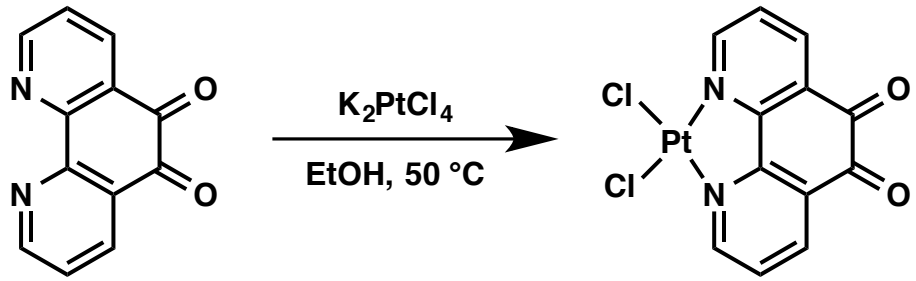

Scheme 5.3 Synthesis of [$PtCl_2$(phendione)], where phendione = 1,10-phenanthroline-5,6-dione.

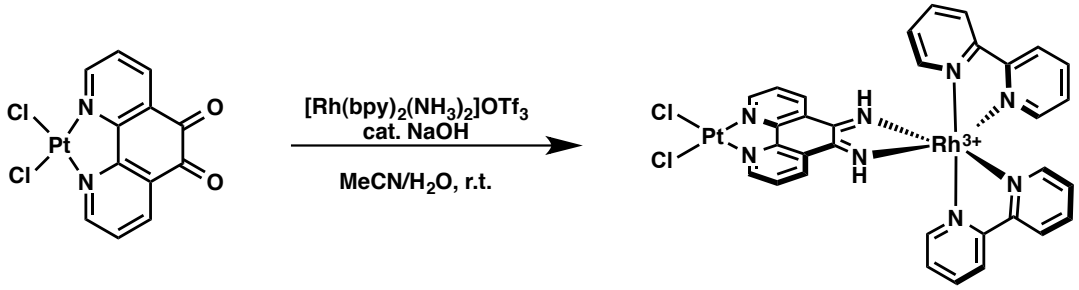

Scheme 5.4 Synthesis of $[(bpy)_2Rh(\mu\text{-phendione})PtCl_2]^{3+}$.

Hz, 2H), 8.44-8.41 (m, 1H), 8.16 (td, *J* = 7.9, 1.4 Hz, 1H), 8.10 (td, *J* = 7.9, 1.3 Hz, 1H), 8.01 (dddd, *J* = 10.1, 7.5, 5.7, 1.4 Hz, 2H), 7.62 (ddt, *J* = 5.9, 1.4, 0.7 Hz, 1H), 7.59 (ddt, *J* = 5.9, 1.5, 0.7 Hz, 1H), 7.41 (ddd, *J* = 7.4, 5.8, 1.4 Hz, 1H), 7.43 (ddd, *J* = 7.5, 5.9, 1.4 Hz, 1H). UV-vis (H_2O, pH 7.0 (**Figure 5.3**) 337 nm (10330 M^{-1} cm^{-1}), 380 nm (2210 M^{-1} cm^{-1}). ESI-MS (cation) *m/z* calc 444 ($M - H^{2+}$), obs. 467 ($M - 2H + Na^{2+}$).

5.2.3.3 $[Rh(bpy)_2bzp]^{3+}$ (Scheme 5.5)

To a 100 ml roundbottom flask was added bzp (15 mg, 0.057 mmol) and $[Rh(bpy)_2(NH_3)_2]OTf_3$ (51 mg, 0.057 mmol) in 40 ml 1:1 H_2O/MeCN. The mixture was basified to pH 13 with 1N NaOH, which imparted a color change from yellow to orange. The reaction was allowed to stir at room temperature. After 24h, the reaction was neutralized with 1N HCl and dried *in vacuo*. The complex was purified via passage through a Sep-pak C18 cartridge (Waters) eluting with 1:1 H_2O/MeCN containing 0.1% TFA. ^{1}H NMR (500 MHz, Deuterium Oxide) δ 10.04 (s, 1H), 9.53 (s, 1H), 9.12 – 8.97 (m, 1H), 8.96 – 8.89 (m, 1H), 8.74 – 8.67 (m, 2H), 8.65 (dd, *J* = 8.3, 6.6 Hz, 1H), 8.61 – 8.55 (m, 1H), 8.54 – 8.50 (m, 1H), 8.42 (t, *J* = 8.0 Hz, 1H), 8.32 (qd, *J* = 7.8, 1.4 Hz, 1H), 8.18 (td, *J* = 7.9, 1.4 Hz, 1H), 8.05 (ddd, *J* = 7.5, 5.7, 1.4 Hz, 1H), 7.98 (s, 1H), 7.81 (m, 2H), 7.73 (m, 1H), 7.69 – 7.65 (m, 1H), 7.63 – 7.57 (m, 1H), 7.55 – 7.51 (m, 1H), 7.43 (ddd, *J* = 7.4, 5.8, 1.3 Hz, 1H), 7.15 (m, 1H), 7.04 (dd, *J* = 3.6, 1.9 Hz, 1H), 6.96 – 6.89 (m, 1H). UV-vis (H_2O, pH 7.0, **Figure 5.4**): 246 nm (113,000 M^{-1} cm^{-1}), 313 nm (59,900 M^{-1} cm^{-1}), 350 nm (38,500 M^{-1} cm^{-1}). ESI-MS (cation): *m/z* calc 671 ($M - 2H^+$), 336 ($M - H^{2+}$), 670.9 obs.

5.2.3.4 $[(bpy)_2Rh(\mu\text{-}bzp)PtCl_2]^{3+}$ (Scheme 5.6)

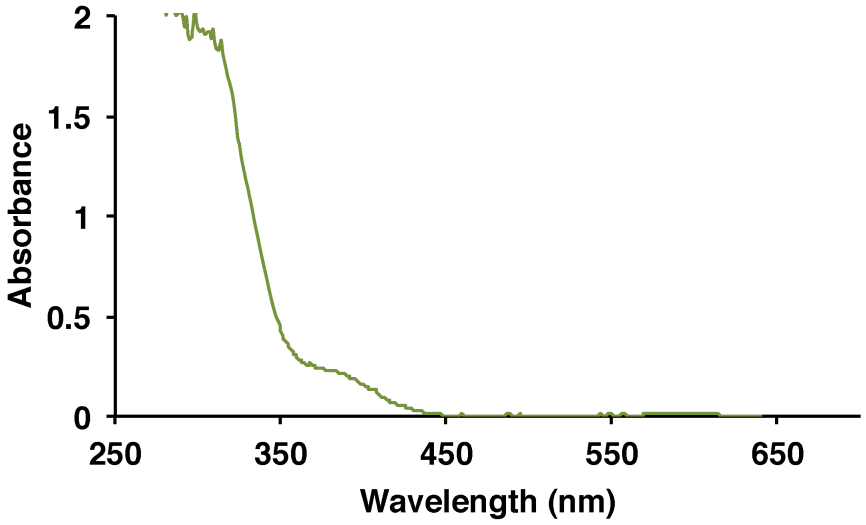

Figure 5.3 UV-visible spectrum of $[(bpy)_2Rh(\mu\text{-phendione})PtCl_2]^{3+}$ in H_2O at pH 7.

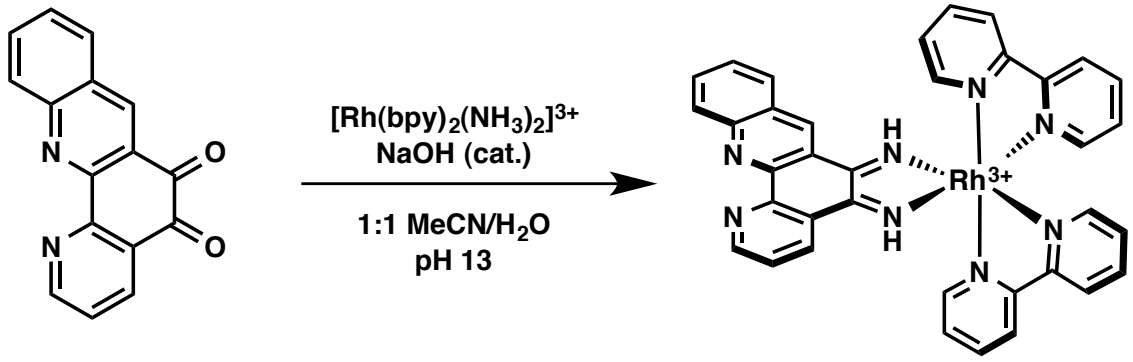

Scheme 5.5 Synthesis of $[Rh(bpy)_2bzp]^{3+}$.

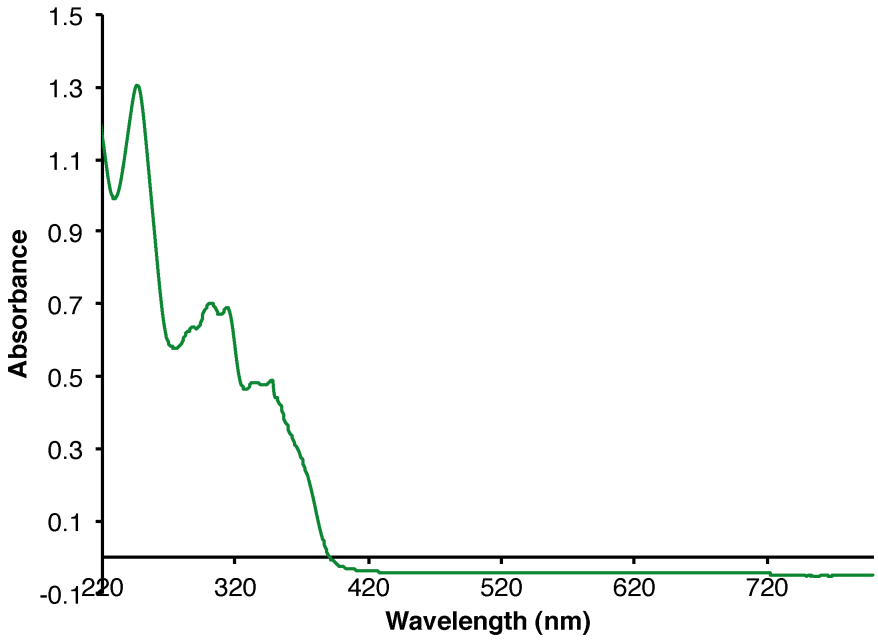

Figure 5.4 UV-visible spectrum of $[Rh(bpy)_2bzp)]^{3+}$ in H_2O at pH 7.

To a 250 ml round-bottomed flask was added $[Rh(bpy)_2bzp]TFA_3$ (60 mg, 0.06 mmol) and K_2PtCl_4 (24.5 mg, 0.06 mmol). The solids were suspended in 50 ml Milli-Q water containing 0.1 ml 1N $HCl_{(aq)}$. The mixture was heated to reflux for 24 h, during which a color change from red to brown was observed. The reaction was filtered, and the filtrate was collected and dried *in vacuo*. The crude residue was dissolved in a minimal volume of ethanol and purified by reverse-phase HPLC. The fractions containing product were identified by ESI-MS, redissolved in water, and subjected to an additional round of HPLC purification. The purified product was dried *in vacuo*, redissolved in water, and loaded onto a QAE Sephadex anion exchange column. $[(bpy)_2Rh(\mu\text{-}bzp)PtCl_2]^{3+}$ was eluted as the chloride salt with 1 M $MgCl_2$. To remove excess $MgCl_2$, the complex was desalted on a SPE column, washed with water, and eluted with methanol. The product was dried immediately to prevent ligand exchange at the platinum center. ^{1}H NMR (D_2O, 500 MHz) δ 9.56 (d, J = 10.7 Hz, 1H), 9.11 (s, 1H), 8.89 – 8.79 (m, 1H), 8.63 (d, J = 8.1 Hz, 1H), 8.60 – 8.50 (m, 4H), 8.48 – 8.42 (m, 1H), 8.38 (dd, J = 14.7, 8.1 Hz, 2H), 8.27 (d, J = 31.9 Hz, 6H), 8.16 – 7.99 (m, 1H), 7.99 – 7.85 (m, 2H), 7.78 (s, 1H), 7.62 (dd, J = 24.4, 5.2 Hz, 1H), 7.54 (s, 1H), 7.49 (s, 1H), 7.44 – 7.24 (m, 1H). ESI-MS (cation): *m/z* 467 ($M - H^{2+}$), 935 ($M - 2H^+$).

5.2.4 DNA Binding Behavior

5.2.4.1 Photocleavage Competition Titration of $[Rh(bpy)_2chrysi]^{3+}$ with $[(bpy)_2Rh(phendione)PtCl_2]^{3+}$

A 17-mer DNA strand (5*'–TTAGGATCATCCATATA–3') (underline denotes the mismatch, asterisk denotes the radiolabel) was labeled with ^{32}P at the 5'-end with [^{32}P]-ATP using polynucleotide kinase (PNK) at 37 °C for 2 h. The radiolabeled DNA

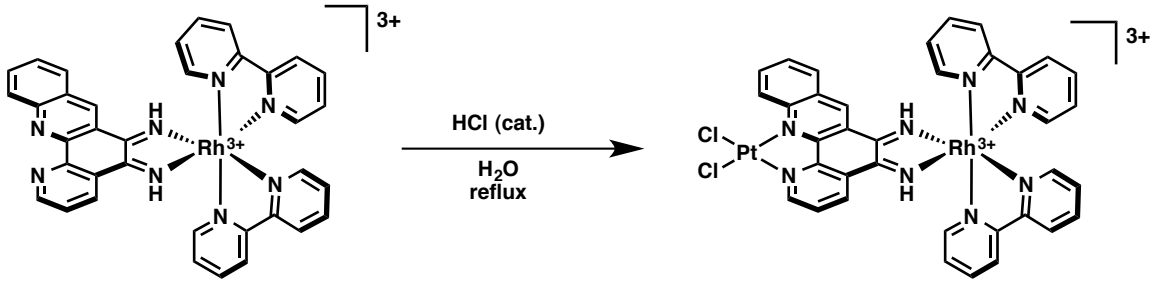

Scheme 5.6 Synthesis of $[(bpy)_2Rh(\mu\text{-}bzp)PtCl_2]^{3+}$.

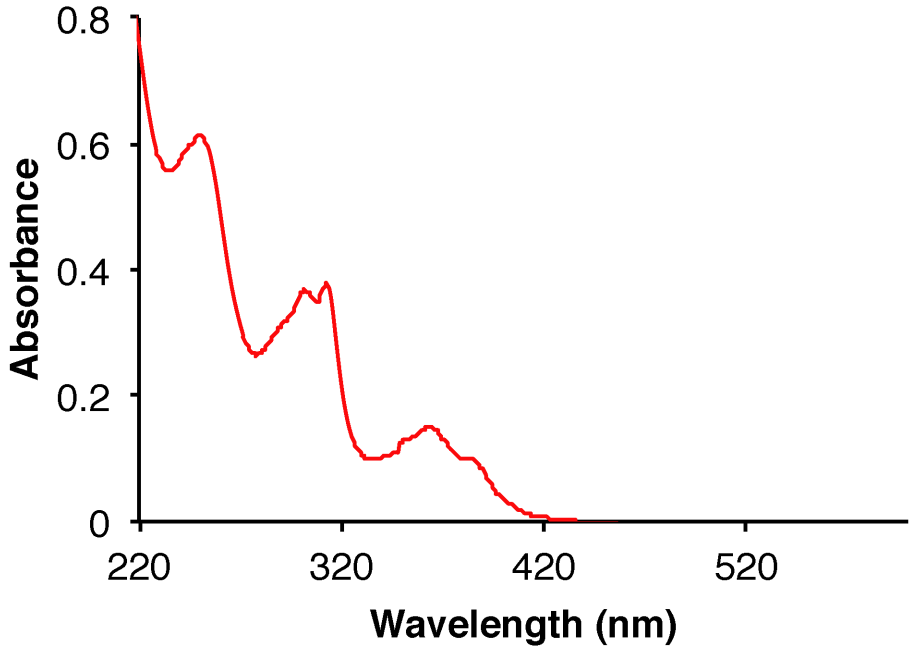

Figure 5.5 UV-visible spectrum of $[(bpy)_2Rh(\mu\text{-}bzp)PtCl_2]^{3+}$ in H_2O at pH 7.

was purified by gel electrophoresis and annealed with its fully matched complement or a complement strand containing a single CC mismatch at the designated site. To prepare samples for gel electrophoresis, 4 μM $[Rh(bpy)_2chrysi]^{3+}$ (5 μL) and varying concentrations (0.5 – 50 μM) of $[(bpy)_2Rh(phendione)PtCl_2]^{3+}$ (5 μL) were added to 2 μM mismatched DNA duplex (10 μL). A light control (10 μL DNA, 10 μL H_2O) and a dark control (10 μL DNA, 5 μL $[Rh(bpy)_2chrysi]^{3+}$, 5 μL $[(bpy)_2Rh(phendione)PtCl_2]^{3+}$, no irradiation) were also prepared. Samples were vortexed and, except for the dark control, irradiated on an Oriel (Darmstadt, Germany) 1000-W Hg/Xe solar simulator (340-440 nm) for 15 min. Samples were then incubated at 37 °C for either 30 min or 2h, dried, then electrophoresed through a 20 % denaturing polyacrylamide gel. The gel was exposed on a phosphor screen and phosphorimaged. The amounts of cleaved and platinated DNA were quantified (ImageQuant), and the fractions of DNA cleaved or platinated were normalized and plotted against the log of the concentration. The data were fit in OriginPro 8.1.

5.2.4.2 Photocleavage Titration of $[(bpy)_2Rh(\mu\text{-bzp})PtCl_2]^{3+}$

A 29mer DNA hairpin with the sequence 5'-GGCAGGCATGGCTTTTTGCCATGCCTGCC -3' was labeled at the 5'-end with [^{32}P]-ATP using polynucleotide kinase (PNK) at 37 °C for 2 h. Mismatched hairpins of the same sequence, but containing either a CC or a GA mismatch at the sites indicated (underline denotes the site where mismatches were inserted) were similarly labeled. The radiolabeled DNA was purified by gel electrophoresis and annealed to by heating to 90 °C in buffer (100 mM NaCl, 20 mM NaP_i, pH 7.1), followed by slow cooling to ambient temperature over 3 h, to give a final concentration of 2 μM hairpin DNA. Racemic

solutions of $[(bpy)_2Rh(\mu\text{-}bzp)PtCl_2]^{3+}$ were prepared in Milli-Q water over a range of concentrations (estimated 1 – 50 μM). For each sample, 2 μM annealed hairpin DNA (10 μl) and $[(bpy)_2Rh(\mu\text{-}bzp)PtCl_2]^{3+}$ at various concentrations (10 μl) were combined to give 1 μM duplex DNA as the final concentration. A "light" control, (ØRh, ØPt) consisting of 2 μM DNA mixed with 10 μl Milli-Q water, and a "dark" control (Ø *hυ*), containing the DNA mixed with the highest concentration of $[(bpy)_2Rh(\mu\text{-}bzp)PtCl_2]^{3+}$ without irradiation, and a positive control, containing 1 μM hairpin DNA containing a CC mismatch and 1 μM *rac*-$[Rh(bpy)_2chrysi]^{3+}$ were also prepared. The samples were vortexed and, except for the dark control, irradiated on an Oriel (Darmstadt, Germany) 1000-W Hg/Xe solar simulator (340-440 nm) for 15 min. The samples were then incubated at 37 °C for 30-60 minutes to promote the formation of covalent platinum adducts and dried under vacuum. The irradiated samples were electrophoresed on a 20% denaturing polyacrylamide gel and exposed to a phosphor screen. The amounts of DNA in each band were analyzed by autoradiography and quantitated by phosphorimagery (ImageQuant).

5.2.4.3 Analysis of DNA Binding

To assess the binding of photocleavage by $[(bpy)_2Rh(\mu\text{-}bzp)PtCl_2]^{3+}$ at the CC mismatch, the fraction of cleaved DNA was quantified and expressed as a percentage of the total DNA in each lane and plotted against the log of the (estimated) concentration of $[(bpy)_2Rh(\mu\text{-}bzp)PtCl_2]^{3+}$ in Origin Pro. DNA platination was analyzed in a similar manner, wherein the fraction of platinated DNA was quantified and expressed as a percentage of the total DNA in each lane and plotted against the log of the concentration of $[(bpy)_2Rh(\mu\text{-}bzp)PtCl_2]^{3+}$.

5.3 Results

5.3.1 Complexes Synthesized

Two bimetallic Rh(III)/Pt(II) DNA binding complexes have been synthesized in which both metal centers are coordinated to a bridging aromatic ligand designed to enter the DNA base stack. One complex employs a 1,10-phenanthroline-5,6-dione ("phendione") intercalating ligand, and the other contains a benzo-fused expanded version of the phendione ligand, benzo[*b*][1,10]phenanthroline-5,6-dione ("bzp"), designed to target thermodynamically destabilized sites in DNA via the metalloinsertive binding mode. The bzp ligand is estimated to be approximately the same width as previously characterized inserting ligands 5,6-chrysenequinone ("chrysi") and benzo[*a*]phenazine-5,6-dione ("phzi"), and thus was anticipated to target destabilized mismatched sites with equal precision.[23-25]

In both complexes, the ligands possess two bidentate coordination sites for each metal center. The di-quinone moiety coordinates to the rhodium center via base-catalyzed imine condensation with a *cis*-diammine rhodium precursor ($[Rh(bpy)_2(NH_3)_2]^{3+}$).[26] Under condensation conditions, no evidence of N-heterocyclic chelation of the rhodium center was observed. Likewise, no chelation of the di-quinone to the platinum center was observed; in the synthesis of both complexes, platinum coordinates exclusively via the phenanthroline nitrogens. This differential coordination strategy affords a facile construction of the bimetallic system in good yields with few side products.

5.3.2 DNA Binding of $[(bpy)_2Rh(phendione)PtCl_2]^{3+}$

5.3.2.1 Binding of $[(bpy)_2Rh(phendione)PtCl_2]^{3+}$ to a CC Mismatch

The DNA binding behavior of $[(bpy)_2Rh(\mu\text{-phendione})PtCl_2]^{3+}$ was characterized using 5'-^{32}P-radiolabeled DNA with the sequence 5'- TTAGGATCATCCATATA-3' and its unlabeled well-matched complement as well as a complement containing a single CC mismatch (underline denotes the mismatch). As it was initially unclear whether or not $[(bpy)_2Rh(\mu\text{-phendione})PtCl_2]^{3+}$ would photocleave the DNA backbone upon binding, titrations were carried out in the absence of $[Rh(bpy)_2chrysi]^{3+}$. Increasing concentrations of the bimetallic complex were incubated with fixed concentrations of DNA and $[Rh(bpy)_2chrysi]^{3+}$, irradiated, and electrophoresed on a 20% denaturing polyacrylamide gel. A representative autoradiogram is shown in **Figure 5.6**. No photocleavage bands are observed for mismatched or well-matched DNA, but evidence of the formation of Pt-DNA crosslinks is visible. The complex exhibits a slight preference for platination of well-matched DNA versus mismatched. **Figure 5.6** also depicts the same gel but with the gain increased, and as such, a small amount of photocleavage can be observed at high concentrations of $[(bpy)_2Rh(\mu\text{-phendione})PtCl_2]^{3+}$ at the site of the mismatch, suggesting that the complex is capable of metalloinsertion. No other photocleavage was evident, so it is unclear from this experiment whether the complex can also intercalate between Watson-Crick base pairs.

The results of the initial photocleavage titration were promising, and so the mismatch recognition capabilities of $[(bpy)_2Rh(\mu\text{-phendione})PtCl_2]^{3+}$ were further characterized by means of a competition titration with $[Rh(bpy)_2chrysi]^{3+}$. A representative autoradiogram is shown in **Figure 5.7**. The fraction of DNA photocleaved

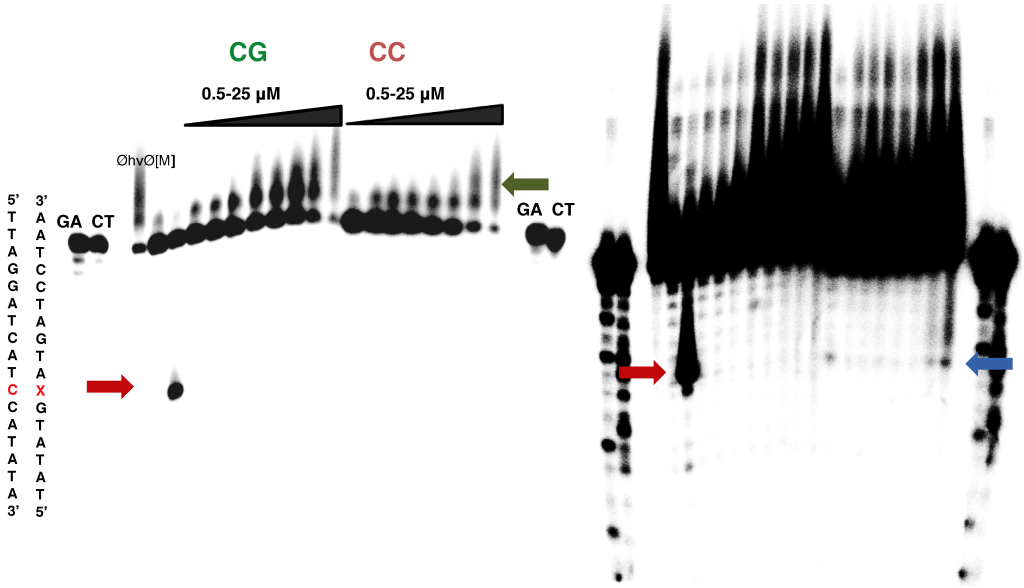

Figure 5.6 Photocleavage titration of $[(bpy)_2Rh(\mu\text{-phendione})PtCl_2]^{3+}$ (0 – 25 μM) on 1 μM 5'-[^{32}P] labeled 17mer duplex DNA with a CC mismatch (denoted by "CC" in red) and a similarly well-matched sequence (denoted by "CG" in green). Samples were irradiated (340-440 nm) for 15 min and electrophoresed on a 20% denaturing polyacrylamide gel. Controls without irradiation (Øhv), and without metal complex (Ø[M]) were included. A control sample of CC-mismatched duplex (1 μM) and $[Rh(bpy)_2chrysi]^{3+}$ (1 μM), which photocleaves DNA at mismatched sites, was also included; the resulting photocleavage product is indicated by the red arrow. The left autoradiogram is the photocleavage titration for both sequences at normal gain; no photocleavage by $[(bpy)_2Rh(\mu\text{-phendione})PtCl_2]^{3+}$ is observed, although the presence of Pt-DNA adducts appear as bands of reduced electrophoretic mobility above the unmodified parent DNA (denoted by the green arrow). The right autoradiogram is the same gel at high gain, and faint photocleavage by $[(bpy)_2Rh(\mu\text{-phendione})PtCl_2]^{3+}$ can be seen at the mismatch (denoted by the blue arrow), but not at well-matched sites.

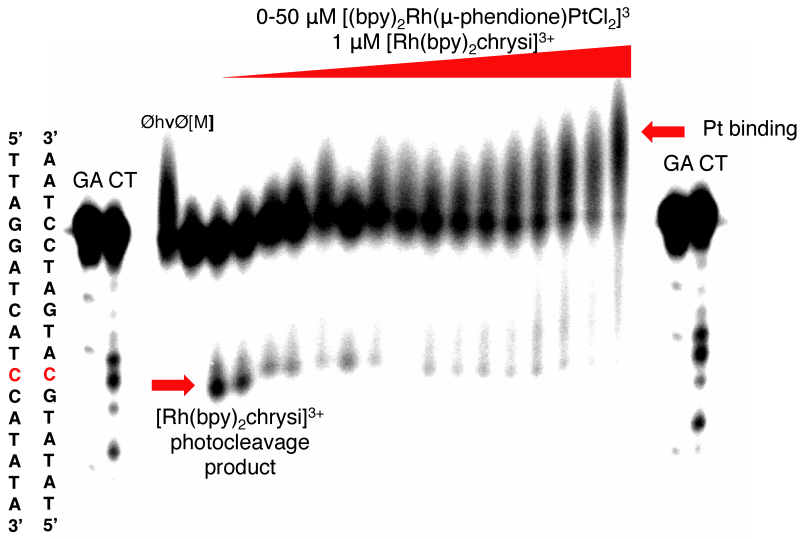

Figure 5.7 Competition titration of increasing concentrations of $[(bpy)_2Rh(\mu\text{-phendione})PtCl_2]^{3+}$ (0-50 μM) with 1 μM *rac*-$[Rh(bpy)_2chrysi]^{3+}$ on 1 μM 5'-[^{32}P] labeled 17mer duplex DNA with a CC mismatch (denoted in red). Samples were irradiated (340-440 nm) for 15 min and electrophoresed on a 20% denaturing polyacrylamide gel. Controls without irradiation (Øhν), and without metal complex (Ø[M]) were included. $[(bpy)_2Rh(\mu\text{-phendione})PtCl_2]^{3+}$ inhibits photocleavage by $[Rh(bpy)_2chrysi]^{3+}$ at the mismatched site. The site of photocleavage by $[Rh(bpy)_2chrysi]^{3+}$ at the mismatch is indicated by an arrow at bands located below the unmodified parent band. Bands of reduced electrophoretic mobility, located above the unmodified parent DNA, are indicative of covalent binding by the platinum subunit.

by $[Rh(bpy)_2chrysi]^{3+}$ at the mismatch decreases with increasing concentrations of the conjugate. It is apparent that the bimetallic complex is fully capable of metalloinsertion at a CC mismatch, although the $[Rh(bpy)_2chrysi]^{3+}$ is never fully outcompeted, even at high concentrations of competitor. Additionally, when the fraction of photocleaved DNA is plotted against the log of the concentration of $[(bpy)_2Rh(\mu\text{-phendione})PtCl_2]^{3+}$ (log[RhPt]), the data do not fit to a sigmoidal curve as is typically observed for photocleavage competition titrations with $[Rh(bpy)_2chrysi]^{3+}$ (**Figure 5.8**).[17] In fact, the data do not fit to any curve from which a binding affinity can be calculated. Likely, this disruption to the equilibrium binding of $[(bpy)_2Rh(\mu\text{-phendione})PtCl_2]^{3+}$ to the mismatch is due to both the complex also performing intercalation at well-matched sites, as well as non-dissociation of the complex from DNA as it becomes covalently bound through the platinum center. Furthermore, distortions to the duplex caused by platinum crosslinking may also interfere with the equilibrium binding constant at the mismatch. Due to the presence of at least two – likely three – simultaneous binding interactions between $[(bpy)_2Rh(\mu\text{-phendione})PtCl_2]^{3+}$ and mismatched DNA (metalloinsertion, platinum crosslinking, and metallointercalation), it is not possible to determine the binding affinity (K_B) of the complex at the mismatch.

5.3.2.2 Covalent Platinum Binding of $[(bpy)_2Rh(phendione)PtCl_2]^{3+}$ to Mismatched and Well-Matched DNA

The formation of platinum-DNA crosslinks was analyzed *in vitro* via gel electrophoresis. Dissociation of the labile chloride ligands from the platinum center in solution enables the formation of covalent platinum adducts with DNA. As can be seen in the autoradiograms in **Figure 5.6** and **Figure 5.7**, platinum binding manifests as bands of

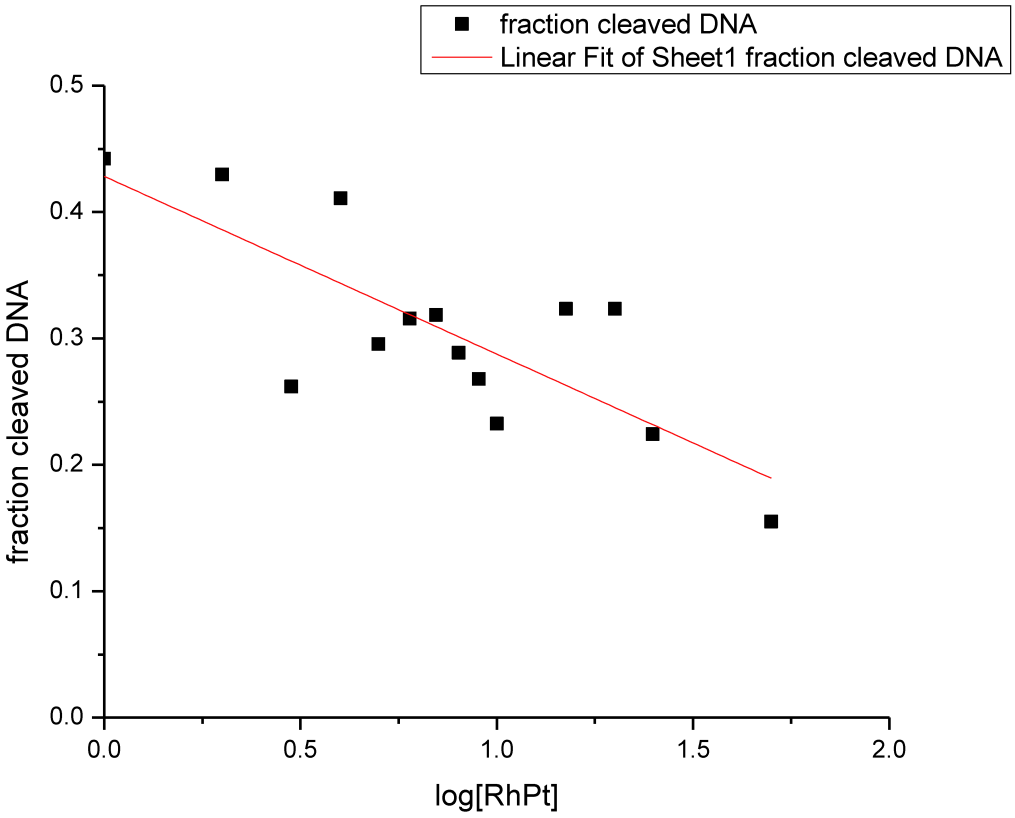

Figure 5.8 Representative plot of photocleavage competition titrations of $[(bpy)_2Rh(\mu\text{-phendione})PtCl_2]^{3+}$ (log [RhPt]) for binding constant determination at the CC mismatch. Experiments were conducted in buffer (50 mM NaCl, 10 mM NaP_i, pH 7.1) using 1 μM duplex DNA and 1 μM rac-$[Rh(bpy)_2chrysi]^{3+,}$ with 0-50 μM $[(bpy)_2Rh(\mu\text{-phendione})PtCl_2]^{3+}$ competitor complex. Although the complex outcompetes $[Rh(bpy)_2chrysi]^{3+}$ at the mismatch, it does not follow the regular sigmoidal dose response curve characteristic of competition titrations, indicating that the equilibrium binding is disrupted. As such, an accurate binding affinity (K_B) for the CC mismatch could not be determined by this method. Data are representative of three independent gels.

reduced electrophoretic mobility, located above the unmodified parent DNA in the denaturing PAGE gel. In the comparison of platinum binding to mismatched versus well-matched duplex, a preference for covalent modification of well-matched DNA is apparent.

The fraction of platinated DNA by $[(bpy)_2Rh(phendione)PtCl_2]^{3+}$ was also explored as a function of both concentration and incubation time. Mismatched DNA was irradiated with varying concentrations of complex (0 – 50 μM) for 15 min and incubated at 37 °C for either 30 min or 2 h. Samples were electrophoresed on a denaturing 20% polyacrylamide gel. The fraction of platinated DNA was quantified and plotted against the log of the concentration of metal complex. After 30 min. incubation, the fraction of Pt-DNA are plotted as a sigmoidal curve, and the percentage of platinated DNA never exceeded 100% (**Figure 5.9**), implying stoichiometric Pt:DNA binding. This behavior resembles the platinum binding characteristics of previous Rh-Pt metalloinsertor conjugates. However, platination interferes with determination of equilibrium binding.

At longer incubations, platinum crosslinking deviates significantly from previously observed behavior. As can be seen in the plot of the percentage of platinated DNA as a function of $[(bpy)_2Rh(phendione)PtCl_2]^{3+}$ concentration, the fraction of bound DNA increases exponentially with concentration (**Figure 5.10**). At the highest concentration (50 μM metal complex) covalent binding exceeds 6:1 Pt:DNA ratio with no evidence of saturation. This curious platination behavior may be due in part to potential intercalation of the complex at several sites within the helix.

5.3.3 DNA Binding of $[(bpy)_2Rh(\mu\text{-}bzp)PtCl_2]^{3+}$

5.3.3.1 Binding of $[(bpy)_2Rh(\mu\text{-}bzp)PtCl_2]^{3+}$ to a CC Mismatch

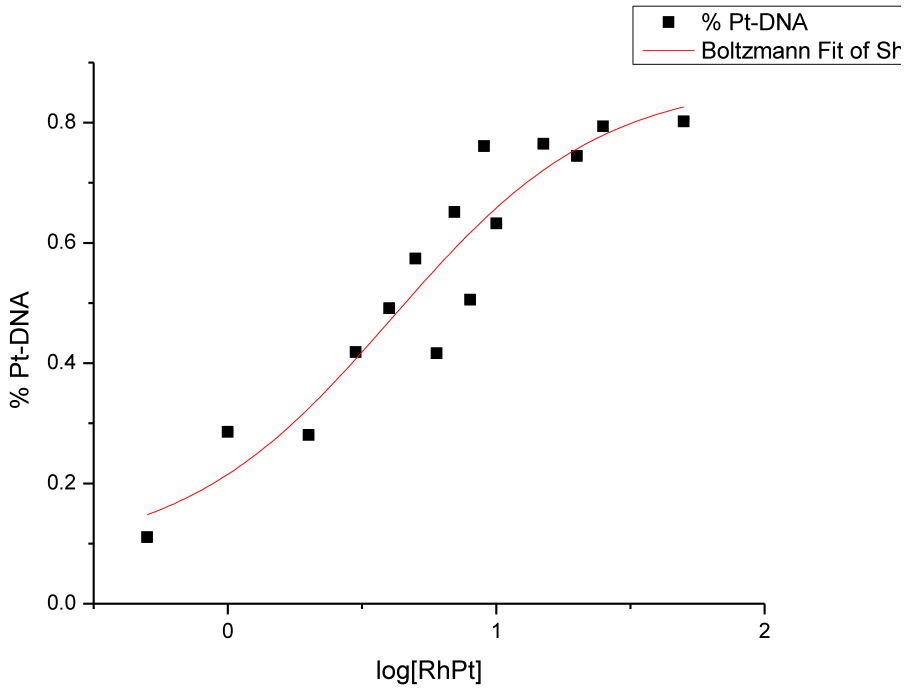

Figure 5.9 Representative sigmoidal curve fit of DNA platination by the platinum subunit of $[(bpy)_2Rh(phendione)PtCl_2]^{3+}$, from 0-50 μM (log [RhPt]). $[(bpy)_2Rh(phendione)PtCl_2]^{3+}$ was incubated with duplex DNA containing a CC mismatch and a d(GpG) site at 37 °C for 30 min to promote the formation of covalent Pt-DNA adducts. Samples were electrophoresed on a 20% denaturing PAGE gel. The amount of platinated DNA is expressed as a fraction of the total DNA in each sample (%Pt-DNA). Data are representative of three independent gels.

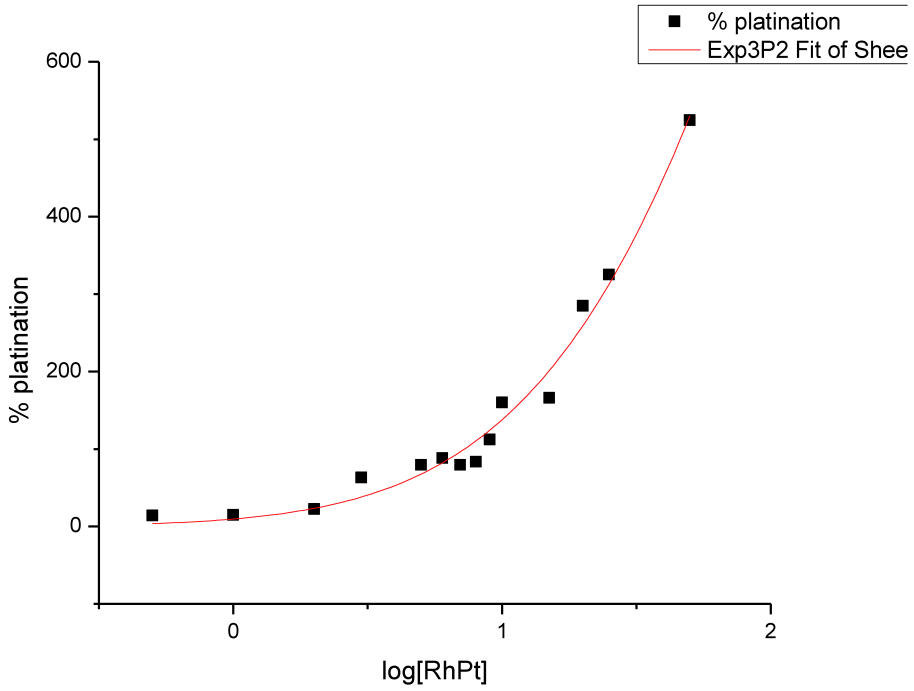

Figure 5.10 Representative exponential curve fit of DNA platination by the platinum subunit of $[(bpy)_2Rh(phendione)PtCl_2]^{3+}$, from 0-50 μM (log [RhPt]). $[(bpy)_2Rh(phendione)PtCl_2]^{3+}$ was incubated with duplex DNA containing a CC mismatch and a d(GpG) site at 37 °C for 2h to promote the formation of covalent Pt-DNA adducts. Samples were electrophoresed on a 20% denaturing PAGE gel. The amount of platinated DNA is expressed as a fraction of the total DNA in each sample (%Pt-DNA). After a 2h incubation period, a 6-fold excess of platinated DNA was observed compared to the 30 minute incubation period. Data are representative of three independent gels.

The DNA binding of $[(bpy)_2Rh(\mu\text{-}bzp)PtCl_2]^{3+}$ was analyzed with a 5'-end radiolabeled 29mer DNA hairpin containing a single CC mismatch of the sequence 5'-GGCAGGCATGGCTTTTTGCCATGCCTGCC -3' (underline denotes the mismatch) (**Figure 5.11**). A band of increased electrophoretic mobility appears at the mismatched site for samples that were irradiated in the presence of the complex, indicating photocleavage at the CC mismatch. This is confirmed by comparison to the positive control, wherein the DNA hairpin is irradiated in the presence of first-generation metalloinsertor $[Rh(bpy)_2chrysi]^{3+}$, which photocleaves DNA on the sugar-phosphate backbone at the site of the mismatch.[23] These results are in contrast with the weak photocleavage observed for the $[(bpy)_2Rh(phendione)PtCl_2]^{3+}$ intercalator analogue. Surprisingly, whereas $[Rh(bpy)_2chrysi]^{3+}$ has previously been shown to exhibit increased photocleavage product with increasing concentrations against a fixed level of DNA – suggestive of enhanced photocleavage efficiency as a result of DNA binding[23-25] – the photocleavage band *decreases* with increasing concentration of $[(bpy)_2Rh(\mu\text{-}bzp)PtCl_2]^{3+}$. Furthermore, the appearance of platinum-DNA crosslinks, represented as bands of reduced electrophoretic mobility located above the unmodified parent bands in the audoradiogram, *increases* as a function of $[(bpy)_2Rh(\mu\text{-}bzp)PtCl_2]^{3+}$ concentration, as expected. Quantification of the bands representing rhodium and platinum binding as a function of metalloinsertor concentration is depicted in **Figure 5.12**. Here, it appears that platinum DNA crosslinking and metalloinsertive photocleavage at a mismatch are inhibitory, rather than complementary. Furthermore, the fraction of photocleaved DNA (as well as the fraction of platinated DNA) do not follow a sigmoidal curve pattern when plotted against concentration, similar to the behavior that was observed for the

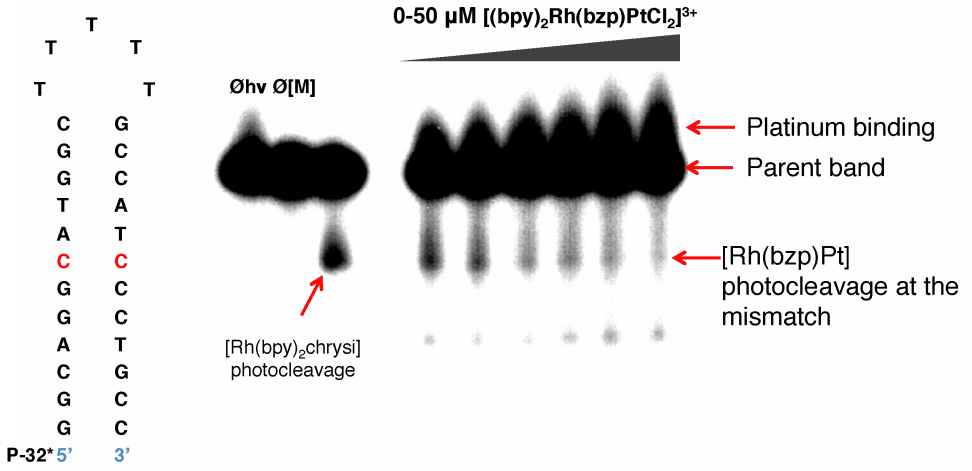

Figure 5.11 Photocleavage titration of $[(bpy)_2Rh(\mu\text{-}bzp)PtCl_2]^{3+}$ (0 – 50 μM) on 1 μM 5'-[^{32}P] labeled 29mer hairpin DNA with a CC mismatch (denoted by "CC" in red). Samples were irradiated (340-440 nm) for 15 min and electrophoresed on a 20% denaturing polyacrylamide gel. Controls without irradiation (Øhν), and without metal complex (Ø[M]) were included. A control sample of CC-mismatched duplex (1 μM) and $[Rh(bpy)_2chrysi]^{3+}$ (1 μM), which photocleaves DNA at mismatched sites, was also included; the resulting photocleavage product is indicated by the red arrow. Photocleavage at the CC mismatch by $[(bpy)_2Rh(\mu\text{-}bzp)PtCl_2]^{3+}$ can also be observed (indicated by the "Rh(bzp)Pt" arrow); however, this photocleavage unexpectedly *decreases* with increasing concentration of complex. The formation of Pt-DNA adducts is also observed, indicated by bands of reduced electrophoretic mobility above the unmodified parent DNA. Platinum binding increases with increasing concentration of $[(bpy)_2Rh(\mu\text{-}bzp)PtCl_2]^{3+}$.

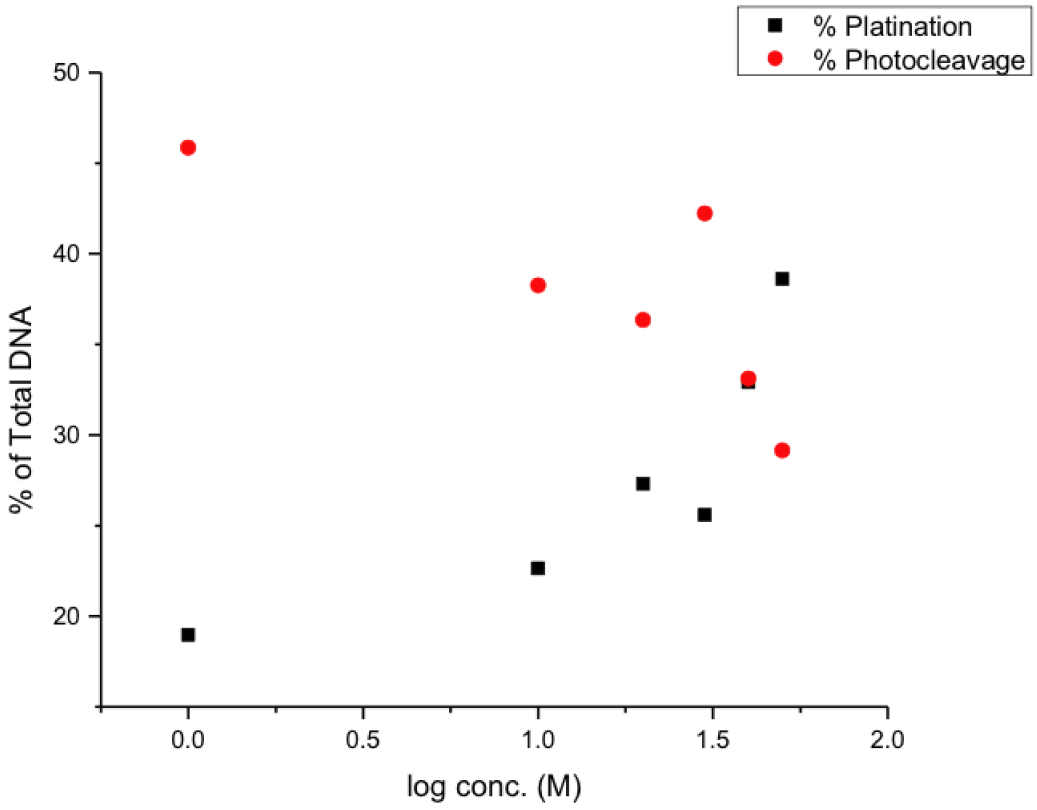

Figure 5.12 Quantification of the percentage of DNA containing a CC mismatch (1 μM) that is photocleaved (red circles) by $[(bpy)_2Rh(\mu\text{-}bzp)PtCl_2]^{3+}$ as a function of complex concentration (0 – 50 μM) after irradiation (340-440 nm) for 15 min followed by electrophoresis on a 20% denaturing polyacrylamide gel. The black squares represent the percentage of platinated DNA under the same conditions. Each point is expressed as the percentage of either photocleavage or platination product relative to the total DNA in each lane. The fraction of photocleaved DNA decreases, while the fraction of platinated DNA increases, implying that the two processes impede one another.

bimetallic intercalator complex. Consequently, reliable a K_B binding constant cannot be calculated for this mismatched site. Finally, it should be noted that, in addition to photocleavage at the mismatched site, additional photocleavage products also appear in the autoradiogram, albeit to a lesser degree than the mismatch photocleavage product, suggestive of non-specific binding interactions.

5.3.3.2 Binding of $[(bpy)_2Rh(\mu\text{-}bzp)PtCl_2]^{3+}$ to a GA Mismatch

Although the inhibitory relationship between mismatch recognition and platinum crosslinking for $[(bpy)_2Rh(\mu\text{-}bzp)PtCl_2]^{3+}$ was unexpected, the complex still displays moderately selective photocleavage at the site of a CC mismatch. We examined the behavior of the complex in the presence of a less thermodynamically destabilized mismatch, such as a GA site. The binding titration was carried out as described above, and the resulting audoradiogram is shown in **Figure 5.13**. Here, photcleavage does not occur at the mismatched site; however, photocleavage products can be seen at other sites throughout the sequence, primarily at purine residues (although, notably, photocleavage does *not* occur at the purine-purine mismatch). Unlike photocleavage at a CC mismatch, this nonspecific strand scission does appear to increase as a function of metalloinsertor concentration, as does the formation of Pt-DNA crosslinks, suggesting that photocleavage and platination occur concomitantly. It is curious that these alternative binding modes are observed, since the purported width of the bzp inserting ligand should preclude nonspecific intercalation. It is possible that partial intercalation, involving side-on binding of the complex to DNA, occurs in the absence of a sufficiently destabilized site and is facilitated by platinum binding. Furthermore, these nonspecific photocleavage bands are not inhibited by the increased platination; rather, photocleavage and covalent

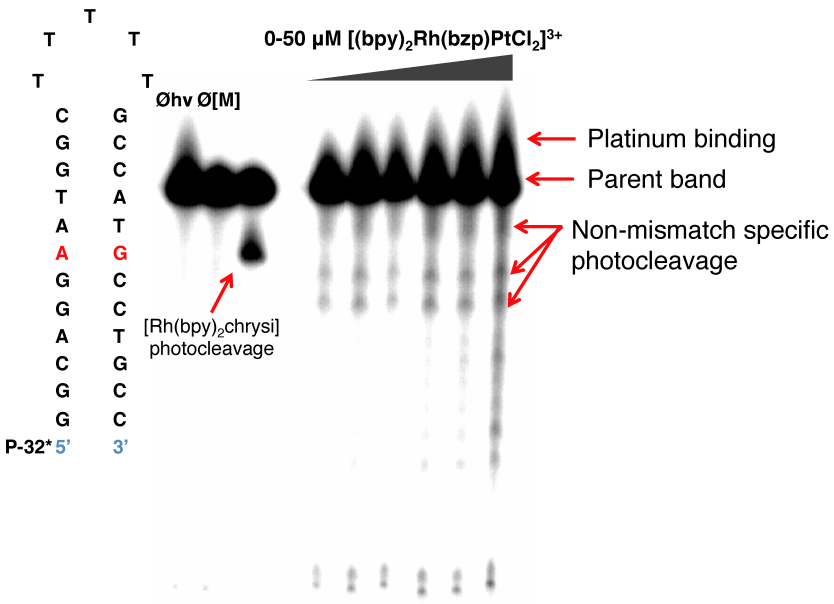

Figure 5.13 Photocleavage titration of $[(bpy)_2Rh(\mu\text{-}bzp)PtCl_2]^{3+}$ (0 – 50 μM) on 1 μM 5'-[^{32}P] labeled 29mer hairpin DNA with a GA mismatch (denoted by "GA" in red). Samples were irradiated (340-440 nm) for 15 min and electrophoresed on a 20% denaturing polyacrylamide gel. Controls without irradiation (Øhν), and without metal complex (Ø[M]) were included. A control sample of CC-mismatched duplex (1 μM) and $[Rh(bpy)_2chrysi]^{3+}$ (1 μM), which photocleaves DNA at mismatched sites, was also included; the resulting photocleavage product is indicated by the red arrow. Nonspecific photocleavage at purines by $[(bpy)_2Rh(\mu\text{-}bzp)PtCl_2]^{3+}$ can be observed; however, this photocleavage increases with increasing concentration of complex. The formation of Pt-DNA adducts is also observed, indicated by bands of reduced electrophoretic mobility above the unmodified parent DNA. Platinum binding also increases with increasing concentration of $[(bpy)_2Rh(\mu\text{-}bzp)PtCl_2]^{3+}$.

platinum binding concurrently increase with increasing concentration of the complex. The oppositional nature of photocleavage and platination, it would seem, is reserved exclusively for the recognition of thermodynamically destabilized mismatches by metalloinsertion.

5.3.3.3 Binding of $[(bpy)_2Rh(\mu\text{-}bzp)PtCl_2]^{3+}$ to Mismatched and Well-Matched DNA Hairpins

Finally, to assess whether the complex exhibits any selective DNA binding, the complex was irradiated in the presence of DNA hairpins that were either fully matched or containing a single CC mismatch. As can be seen in **Figure 5.14**, the binding of $[(bpy)_2Rh(\mu\text{-}bzp)PtCl_2]^{3+}$ to the well-matched hairpin strongly resembles that of the hairpin containing a GA mismatch (**Figure 5.13**) – that is, the complex photocleaves at the same residues (which appear to the guanine residues) in both sequences in the absence of a thermodynamically destabilized site. Furthermore, this photocleavage pattern is concentration-dependent and concomitant with platinum binding. In the presence of a CC-mismatched hairpin, however, photocleavage at the destabilized mismatched site is largely independent of complex concentration and the extent of platinum-DNA crosslinks. Furthermore, the photocleavage products observed in the presence of well matched or GA-mismatched DNA are largely absent in the CC-mismatched sequence. It is possible that metalloinsertion at a mismatch precludes the formation of nonspecific photodamage products; some minor photodamage can be observed at well-matched sites, although these products appear to a much lesser degree than cleavage at the mismatch. As a result, the bimetallic $[(bpy)_2Rh(\mu\text{-}bzp)PtCl_2]^{3+}$

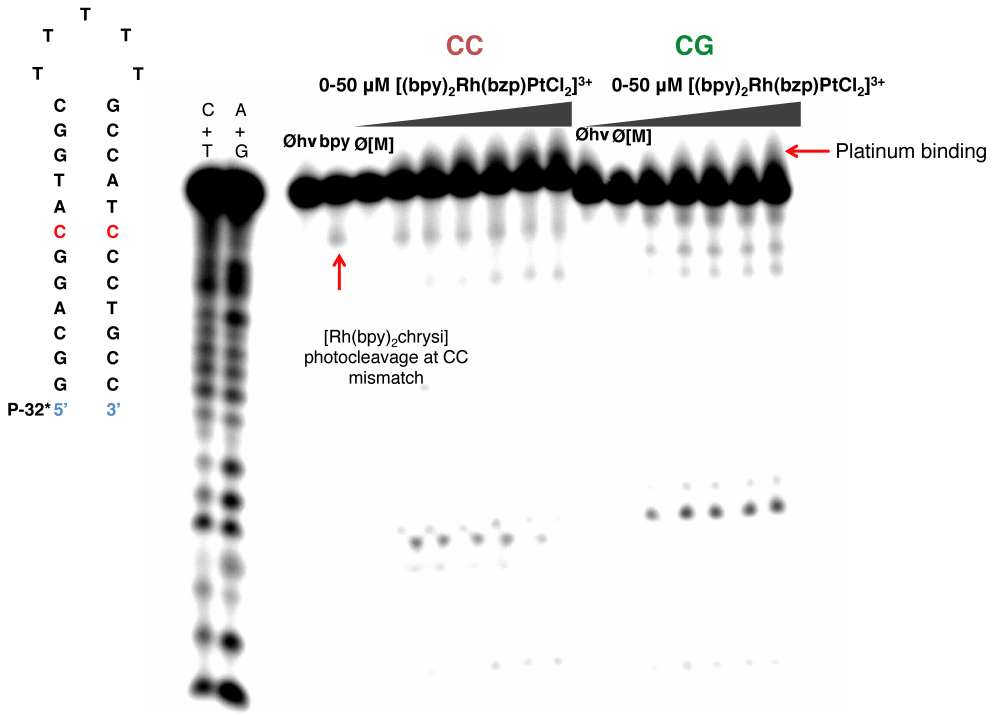

Figure 5.14 Photocleavage titration of $[(bpy)_2Rh(\mu\text{-}bzp)PtCl_2]^{3+}$ (0 – 50 μM) on 1 μM 5'-[^{32}P] labeled 29mer hairpin DNA with a CC mismatch (denoted by "CC" in red) and a similarly well-matched sequence (denoted by "CG" in green). Samples were irradiated (340-440 nm) for 15 min and electrophoresed on a 20% denaturing polyacrylamide gel. Maxam-Gilbert sequencing lanes (C+T and A+G) are shown on the left. Controls without irradiation (Øhν), and without metal complex (Ø[M]) were included. A control sample of CC-mismatched duplex (1 μM) and $[Rh(bpy)_2chrysi]^{3+}$ (1 μM), which photocleaves DNA at mismatched sites, was also included; the resulting photocleavage product is indicated by the red arrow. As shown previously in **Figure 5.11**, the complex photocleaves at the CC mismatch. In the presence of well-matched DNA, the complex behaves as in **Figure 5.13**, performing nonspecific photocleavage. For both CC-mismatched and well-matched sequences, platination (indicated by the arrow) increases with concentration.

complex displays distinctive binding modes that appear to depend on the thermodynamic stability of the nucleic acid duplex.

The percentages of platinated DNA for mismatched and well matched sequences were quantified and the results are shown in **Figure 5.15**. The complex displays little preferential binding for either type of DNA – if anything, a slight preference for well-matched DNA is observed. However, the effects of irradiation with long-wave UV light (340-440 nm) appear to have profound effects on platination levels for mismatched DNA, but not for well-matched (**Figure 5.16**). In the absence of irradiation, platination of well-matched DNA remains unchanged. For the CC-mismatched hairpin, however, platination is significantly attenuated in the dark, but is enhanced to levels similar to that of well-matched DNA upon irradiation. Although the photosensitivity of platinum complexes is known,[27] the light-dependence of platinum binding for mismatched DNA, but not well-matched (and, presumably, GA-mismatched DNA), serves to further confirm that at least two distinct binding modes exist for $[(bpy)_2Rh(\mu\text{-}bzp)PtCl_2]^{3+}$, depending on the thermodynamic stability of the DNA to which it binds.

5.4 Discussion

The complexes described herein are comprised of two metal centers coordinated to a planar aromatic ligand that interacts with the nucleobase π-stack of DNA. Two structural analogues were synthesized, one containing an intercalating phendione ligand, while the other incorporated a sterically expanded analogue of phendione that was anticipated to target DNA mismatches through metalloinsertion. In both cases, injection of the bridging ligand into the helix is intended to situate the square planar platinum (II) center directly in the helix at the point of intercalation/insertion, while the distally

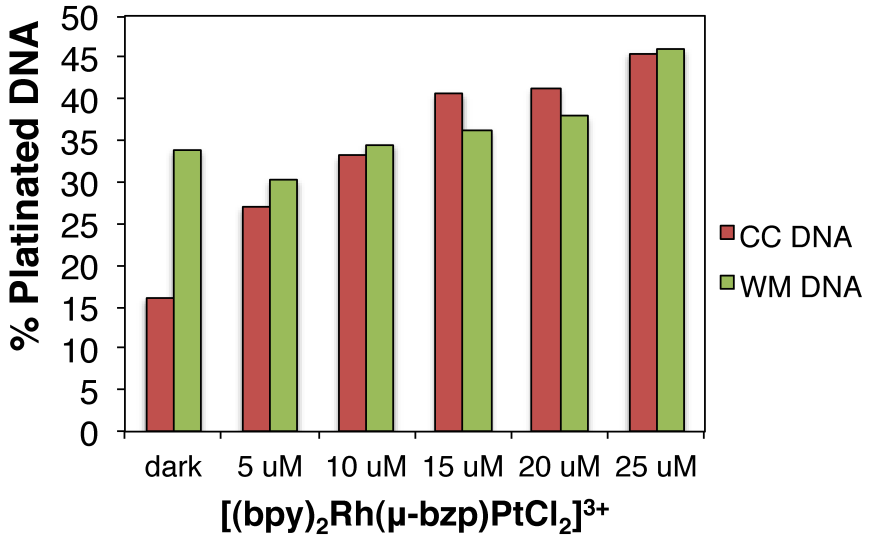

Figure 5.15 Quantification of the percentage of hairpin DNA containing a CC mismatch (red) or is fully matched (green) (1 μM) that is platinated by $[(bpy)_2Rh(\mu\text{-}bzp)PtCl_2]^{3+}$ as a function of complex concentration (0 – 50 μM) after irradiation (340-440 nm) for 15 min (except for the dark control, "dark") followed by electrophoresis on a 20% denaturing polyacrylamide gel. Each point is expressed as the percentage of either photocleavage or platination product relative to the total DNA in each lane. Little difference in platinum crosslinking is observed for mismatched versus well-matched DNA, except in the absence of irradiation, where platinum binding of mismatched DNA is significantly attenuated. Data are representative of three independent gels.

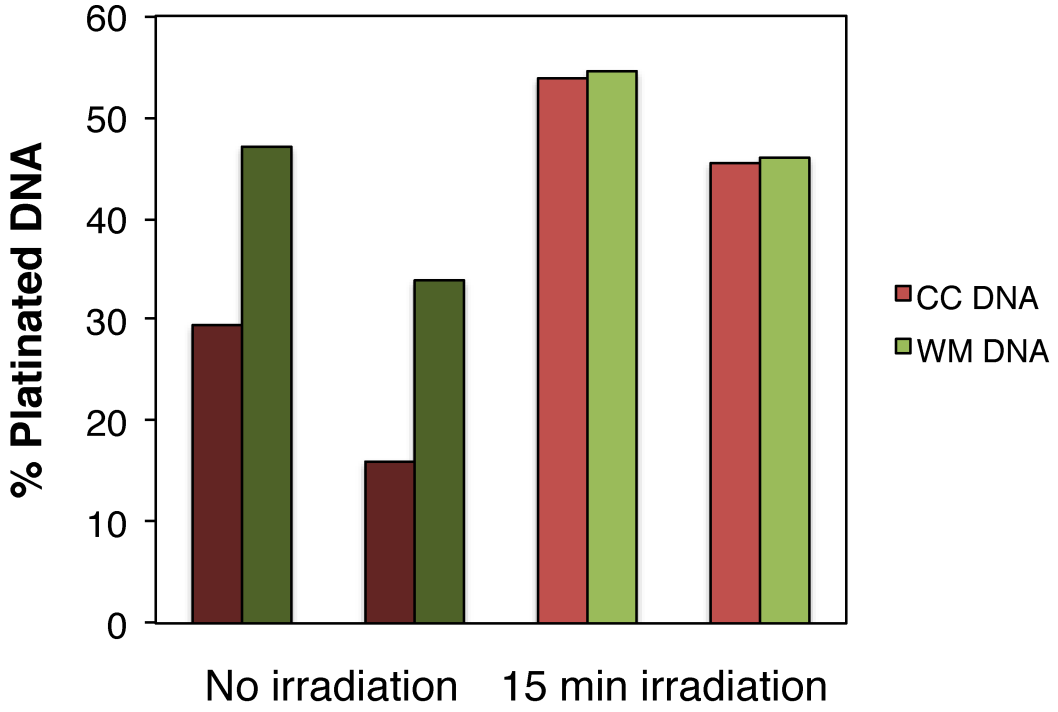

Figure 5.16 Quantification of the percentage of platinated CC-mismatched ("CC DNA," red) and well-matched ("WM DNA," green) hairpin DNA by $[(bpy)_2Rh(\mu\text{-}bzp)PtCl_2]^{3+}$ (50 μM) either in the absence of irradiation (dark red and dark green for CC and WM DNA, respectively) or after 15 min irradiation (340-440 nm) (light red and light green for CC and WM DNA, respectively). Platination of mismatched DNA is attenuated in the absence of light, but irradiation has little effect on the binding of well-matched DNA.

coordinated octahedral rhodium center resides in the groove. This design contrasts with well-studied examples of dinuclear DNA binding complexes, which typically involve two inert centers (usually ruthenium (II)) that both contain sterically bulky ancillary ligands.[28,29] Complexes of this nature are bridged by lengthy intercalating ligands and purportedly bind DNA through a kinetically slow "threading" mechanism that involves passing the bulky ancillary substituents through the base stack through severe DNA distortions.[30] The square planar *cis*-dichloroplatinum (II) moiety is quite flat by comparison, even with the relatively large platinum and chlorine atoms, and we considered it more likely to fit into the base stack.

DNA binding experiments have demonstrated that, in the presence of the mismatch, both the bridging intercalating and inserting ligands can successfully insert into the helix, as evidenced by the competitive displacement of the $[Rh(bpy)_2chrysi]^{3+}$ at a CC mismatch. This also implies that both complexes bind the mismatched sites from the minor groove of DNA. The defining characteristic of the metalloinsertion binding mode, the ejection of the mismatched bases from the duplex to make room for the expansive incoming ligand,[31-34] likely also facilitates accommodation of the platinum substituent in the helix. However, the presence of the platinum center severely disrupts the apparent equilibrium of metalloinsertion for both complexes, as is evidenced by the irregular competition titration curves. It is unclear whether this is due to the formation of covalent platinum adducts, or due to the mere presence of the relatively sizeable platinum center in the base stack. It is potentially a combination of these two factors; threading intercalator complexes, for instance, display substantially reduced association and dissociation rates compared to their monomeric analogues.[30] Previously characterized

conjugates where the platinum is appended to a rhodium ancillary ligand have not demonstrated such interference with the binding affinity for a mismatch through the covalent coordination of DNA.[3,5]

It was less apparent from these experiments whether the phendione complex is also able to intercalate into the duplex at Watson-Crick base pairs. The unusual platinum binding behavior at long incubation period, however, has never been observed for previous metalloinsertor-platinum conjugates – a six fold excess of platinum binding to DNA does not occur for these complexes even in 50-100 fold excess concentrations, due to duplex distortions incurred by crosslinked platinum that preclude the coordination of additional equivalents.[5] Indeed, even the $[(bpy)_2Rh(\mu\text{-}bzp)PtCl_2]^{3+}$ analogue does not display this platination efficiency. It is possible that the intercalation of multiple equivalents of $[(bpy)_2Rh(phendione)PtCl_2]^{3+}$ stabilizes and rigidifies the duplex, enabling the coordination of extremely high platinum stoichiometries. Additionally, the positioning of the complex upon binding to DNA could affect the rates of crosslinking: metallointercalation from the major groove could potentially favor excessive platinum binding more so than metalloinsertion from the minor groove.

The behavior of the metalloinsertor analogue, $[(bpy)_2Rh(\mu\text{-}bzp)PtCl_2]^{3+}$, is even more unusual. Unlike $[(bpy)_2Rh(phendione)PtCl_2]^{3+}$, the complex displays robust photocleavage of DNA upon long-wave UV irradiation. However, $[(bpy)_2Rh(\mu\text{-}bzp)PtCl_2]^{3+}$ appears to exhibit very different binding modes depending on the thermodynamic stability of the DNA oligonucleotide to which it is bound. In the presence of fully matched DNA or DNA containing a more stabilized mismatch, such as GA, the complex performs photocleavage at several purine residues throughout the sequence.

This photocleavage is dose-dependent and increases concomitantly with increasing platination levels. It is unclear why this photocleavage occurs; it is possible that platination of the DNA at purine residues situates the bzp ligand such that a side-on intercalation of the ligand occurs. In contrast, in the presence of DNA containing a CC mismatch, $[(bpy)_2Rh(\mu\text{-}bzp)PtCl_2]^{3+}$ does photocleave at the destabilized site, but this photocleavage is not concentration-dependent, while platinum binding is. In fact, photocleavage at a mismatch and platinum crosslinking appear to be at odds with one another in the presence of mismatched DNA. It should be noted, however, that the apparent inhibition of photocleavage by platinum binding does not necessarily indicate the inhibition of metalloinsertion at the mismatch; many monomeric rhodium metalloinsertor complexes are known to bind destabilized sites with high affinity even if they do not possess photocleavage ability.[17,19] It is possible that merely the DNA strand scission is attenuated, while the complex is still allowed to bind.

Additional evidence supporting the notion of differential binding of $[(bpy)_2Rh(\mu\text{-}bzp)PtCl_2]^{3+}$ to mismatched versus well-matched DNA is the apparent effect of UV irradiation on platinum crosslinking. In the absence of irradiation, adduct formation at DNA containing a CC mismatch is significantly attenuated, while there is no difference in the platination of well-matched DNA in the presence and absence of UV light. One potential explanation is that irradiation of mismatch-bound complex facilitates photolysis of the platinum center; perhaps the platinum center reacts with the C1' radical that forms at the deoxyribose sugar adjacent to the mismatched site upon metalloinsertor photocleavage.[23-25] This would also explain the apparent light-independence observed with the complex in the presence of well-matched or GA-mismatched sequences, where

metalloinsertion does not occur. If the complex thus encounters a DNA oligomer sequence that precludes metalloinsertion, then the platinum is simply free to crosslink the DNA once it has been thermally or photochemically activated through the displacement of the chloride ligands. **Figure 5.17** depicts a schematic of the proposed differential binding modes for $[(bpy)_2Rh(\mu\text{-}bzp)PtCl_2]^{3+}$ at mismatched and well-matched DNA.

5.5 Conclusions

We have constructed two mixed-metal Rh-Pt complexes, $[(bpy)_2Rh(phendione)PtCl_2]^{3+}$ and $[(bpy)_2Rh(\mu\text{-}bzp)PtCl_2]^{3+}$, wherein the metal centers are bridged by a planar ligand possessing either intercalative or insertive DNA binding capabilities, respectively. These complexes display bifunctional DNA binding properties through both metalloinsertion at thermodynamically destabilized sites in addition to the formation of covalent platinum adducts. In the case of the $[(bpy)_2Rh(phendione)PtCl_2]^{3+}$, a third, intercalative binding mode is also possible. The direct insertion of the platinum metal center into the base stack at the mismatched site imparts major disruptions to the apparent equilibrium binding constant of the rhodium-chrysi moiety at the mismatch. In the case of the $[(bpy)_2Rh(\mu\text{-}bzp)PtCl_2]^{3+}$, the complex exhibits differential binding modes in the presence of mismatched versus well-matched DNA. The presence of a destabilized site alters both the intercalative/insertive properties of the bzp ligand as well as the efficiency of platinum binding. While the intended outcome of this design was the intrinsic linkage of platination to mismatch recognition, the two binding modes are in fact at odds with one another – one binding function inhibits the other at the mismatched site. In addition, these distinctive DNA binding behaviors do not lead to an enhancement of platination of mismatched DNA over well-matched; in fact, both complexes appear to

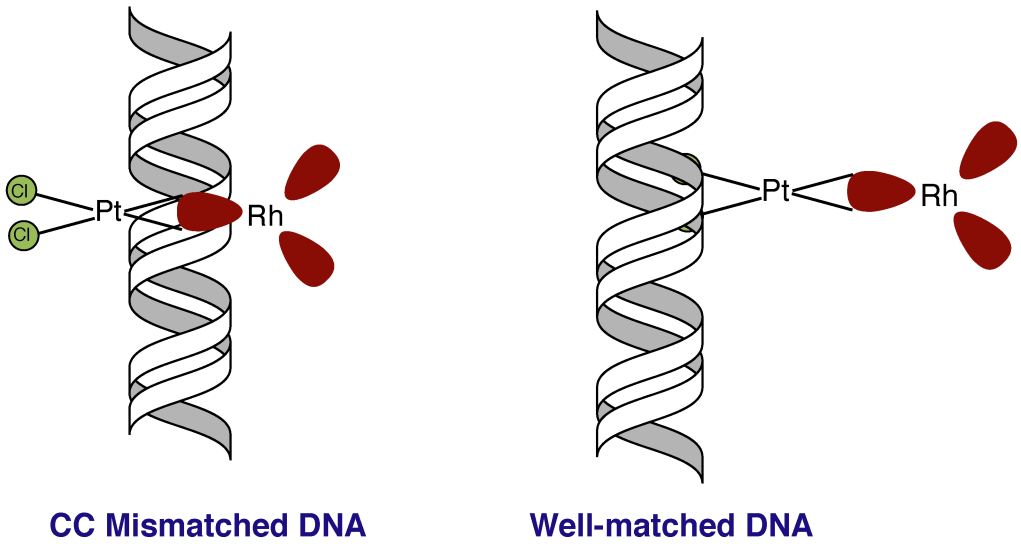

Figure 5.17 Schematic of hypothesized binding interactions of $[(bpy)_2Rh(\mu\text{-}bzp)PtCl_2]^{3+}$ in the presence of mismatched DNA (left) versus well-matched DNA (right). When the complex encounters a destabilized site, the expansive bzp ligand inserts into the duplex, placing the platinum center in the intervening space. It is possible that, upon irradiation, reaction between the resulting deoxyribose radical and the platinum center reduces photocleavage efficiency and releases the platinum, enabling crosslinking. In the absence of a destabilized site, platination of DNA is driven solely by thermal activation of the complex via hydrolysis of the labile chloride ligands.

preferentially bind well-matched DNA. While this likely limits the potential therapeutic applications of these complexes in targeted chemotherapy, the unusual DNA binding properties of these complexes merit further investigation into their biological activity.

5.6 References

1 Schatzschneider, U.; Barton, J. K. *J. Am. Chem. Soc.* **2004**, *126*, 8630−8631.

2 Lim, M. H.; Lau, I. H.; Barton, J. K. *Inorg. Chem.* **2007**, *46*, 9528−9530.

3 Petitjean, A.; Barton, J. K. *J. Am. Chem. Soc.* **2004**, *126*, 14728−14729.

4 Brunner, J.; Barton, J. K. *Biochemistry* **2006**, *45*, 12295−12302.

5 Weidmann, A. G.; Barton, J. K. *Inorg. Chem.* **2014**, *53*, 7812-7814.

6 Mansour, V. H.; Rosenberg, B.; Vancamp, L.; Trosko, J. E. *Nature* **1969**, *222*, 385–386.

7 Wheate, N. J.; Walker, S.; Craig, G. E.; Oun, R. *Dalton Trans.* **2010**, *39*, 8113–8127

8 Kelland, L. R.; Sharp, S. Y.; O'Neill, C. F.; Raynaud, F. I.; Beale, P. J.; Judson, I. R. *J. Inorg. Biochem.* **1999**, *77*, 111–115.

9 Jamieson, E. R.; Lippard, S. J. *Chem. Rev.* **1999**, *99*, 2467-2498.

10 Wang, D.; Lippard, S. J. *Nat. Rev. Drug Discovery* **2005**, *4*, 307–320.

11 Homesley, H. D.; Bundy, B. N.; Hurteau, J. A.; Roth, L. M. *Gynecol. Oncol.* **1999**, *72*, 131-137.

12 Weidmann, A. G.; Komor, A. C.; Barton, J. K. *Comments in Inorg. Chem.***2014,** *34*, 114-123.

13 Weidmann, A. G.; Barton, J. K. *Manuscript in preparation* (See Thesis Chapter 4).

14 Ernst, R. J. *Unpublished results.*

15 Hart, J. R.; Glebov, O.; Ernst, R. J.; Kirsch, I. R.; Barton, J. K. *Proc. Natl. Acad. Sci. U.S.A.* **2006**, *103*, 15359–15363.

16 Karran, P.; Offman, J.; Bignami, M. *Biochimie* **2003**, *85*, 1149-1160.

17 Ernst, R. J.; Song, H.; Barton, J. K. *J. Am. Chem. Soc.* **2009**, *131*, 2359–2366.

18 Ernst, R. J.; Komor, A. C.; Barton, J. K. *Biochemistry* **2011**, *50*, 10919–10928.

19 Komor, A. C.; Schneider, C. J.; Weidmann, A. G.; Barton, J. K. *J. Am. Chem. Soc.* **2012**, *134*, 19223–19233.

20 Weidmann, A. G.; Komor, A. C.; Barton, J. K. *Philos. Trans. R. Soc. A.* **2013**, *371*, 20120117.

21 Weidmann, A. G. *Unpublished results*

22 Roy, S.; Hagen, K. D.; Maheswari, P. U.; Lutz, M.; Spek, A. L.; Reedijk, J.; van Wezel, G. P. *Chem. Med. Chem.* **2008**, *3*, 1427-1434.

23 Jackson, B. A.; Barton, J. K. *J. Am. Chem. Soc.* **1997**, *119*, 12986–12987.

24 Jackson, B. A.; Alekseyev, V. Y.; Barton, J. K. *Biochemistry* **1999**, *38*, 4655–4662.

25 Jackson, B. A.; Barton, J. K. *Biochemistry* **2000**, *39*, 6176–6182.

26 Murner, H.; Jackson, B. A.; Barton, J. K. *Inorg. Chem*. **1998**, *37*, 3007−3012.

27 Bednarski, P. J.; Mackay, F. S.; Sadler, P. J. *Anticancer Agents Med. Chem.* **2007**, *7*, 75-93.

28 Liu, H.-K.; Sadler, P. J. *Acc. Chem. Res.* **2011**, *44*, 349-359.

29 Andersson, J.; Lincoln, P. *J. Phys. Chem. B*, **2011**, *115*, 14768-14775.

30 Nordell, P.; Lincoln, P. *J. Am. Chem. Soc.* **2005**, *127*, 9670-9671.

31 Cordier, C.; Pierre, V. C.; Barton, J. K. *J. Am. Chem. Soc.* **2007**, *129*, 12287–12295.

32 Zeglis, B. M.; Pierre, V. C.; Kaiser, J. T.; Barton, J. K. *Biochemistry* **2009**, *48*, 4247–4253.

33 Pierre, V. C.; Kaiser, J. T.; Barton, J. K. *Proc. Natl. Acad. Sci. U.S.A.* **2007**, *104*, 429–434.

34 Song, H. Kaiser; J. T.; Barton, J. K. *Nature Chem.* **2012**, *4*, 615–620.